Synchronous Lagrangian and Eulerian Velocity Measurements
IEEE SIXTH WORKING CONFERENCE ON CURRENT MEASUREMENT

Jerome A. Smith
Scripps Institution of Oceanography
La Jolla, CA 92093-0213 USA

Abstract— A Phased Array Doppler Sonar (PADS), as developed at SIO, images both acoustic backscatter intensity and Doppler shift over areas up to 90 degrees in bearing by 500 m in range. Sequences of images are recorded continuously for up to two months, with individual "pings" 0.5 to 1.0 seconds apart. The images permit two independent estimates of the mean velocity to be formed over the imaged area: one from the Doppler shift (radial velocity), and another from tracking features from one frame to the next. For grazing incidence, the Doppler shifts provide an essentially Eulerian velocity estimate, an intensity-weighted average from the wave troughs downward. In contrast, the feature-tracking velocities are Lagrangian. A unique aspect of this is that both Eulerian and Lagrangian velocities are estimated from the same data. The difference between these two velocity estimates compares well with the Stokes' drift calculated via linear theory from a resistance wire elevation array.

I. Introduction

With the recognition that the ocean surface layer is infused with a rich variety of structures, appreciation 2-D maps of surface features has grown. Here, estimates of acoustic backscatter intensity and radial velocity are described that are digitally beamformed over a continuous sector, so that (for example) surface waves can be robustly averaged out or analyzed.

A 195 kHz "Phased Array Doppler Sonar" (PADS) was deployed and operated throughout the Marine Boundary Layer Experiment (MBLEX, February-March and April-May 1995). In MBLEX leg 1, it was operated with the beam-formed sector lying horizontally across the surface, mapping the surface over a pie-shaped area roughly 25° wide and 190-450 m in range. This provides a continuous sequence of 2-D images of the radial velocity field at the ocean surface over several weeks; in particular, over a period of strong forcing associated with a gale-force storm. The space-time evolution of surface velocity patterns can be examined unambiguously using such image sequences, over the entire course of the storm. These PADS measurements are the central focus of this paper.

II. Field experiment setting

Leg 1 of the MBLEX took place along a drift track 50 to 100 km offshore of Point Arguello, just north of Point. Conception, California (Fig. 1). For the 2 weeks beginning on February 19, 1995, the Floating Instrument Platform (*Flip*) was moored at 121°W, 34.5°N on a single-point mooring. At 2316 UTC March 6 (year day 65.96) the line was cut, and *Flip* drifted NW for the next week, until the end of operations on March 12.

Wind and Stokes' drift are among primary input parameters for models of Langmuir circulation. Wind stress was estimated from a sonic anemometer mounted directly above a four-wire wave array, facilitating wind-wave correlation studies [1]. Both sonic and wave wire data were corrected for motion of *Flip* [2]. Estimates of the wave-induced Stokes' drift were formed from the four-wire wave array, using surface elevations and tilts as functions of frequency up to 0.5 Hz [3]. The results were converted to Stokes' drift via linear theory, and integrated over the directional-frequency spectrum to estimate the drift at the surface. On March 8 (year day 67) the wind was initially calm (Fig. 2). It increased uniformly from the SE, beginning near 2 m/s at 0600 and reaching 12 m/s by midnight UTC. It remained steady and strong over the next day, finishing March 9 with a steady 15 m/s breeze. These 2 days are the focus period of this study. The wind direction also remained steady from the SE. The wind stress was well behaved in that discrepancies between bulk-formula and eddy-correlation derived estimates of the stress are small (with $C_d \approx .001$).

Vertical profiles of horizontal velocity were also monitored, with uplooking and downlooking Doppler sonar systems mounted at 90 m depth. Sidelobes from the surface hit contaminated estimates within about 20 m of the surface. To make a cross-thermocline shear estimate, surface

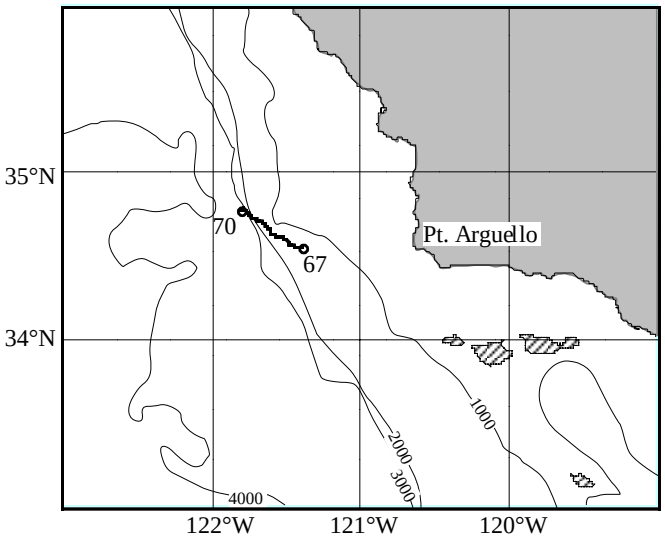

Fig. 1. *Flip*'s track over year days 67 to 70, during MBLEX leg 1. The primary driving force is the average current over the top 90 m of water. Depths are in meters.

velocities from the PADS system were combined with velocity estimates averaged over an intermediate range interval (35-45 m) of the uplooking data.

III. PADS DATA PROCESSING

A. Acoustic Doppler Basics

Pulses of sound are transmitted and reflect off bubbles in the water. The pulses travel outward at the speed of sound, and knowledge of this speed is used to convert the information into functions of range. In a typical system the signal is complex-demodulated such that a zero Doppler shift yields a zero-frequency (complex dc) signal. The temporal rate of change of phase of this demodulated signal yields the mean Doppler shift. This is estimated from the phase of a complex covariance, formed between the demodulated signal at 2 times a small time apart. The magnitude of this same time-lagged complex covariance provides an intensity estimate. The duration of the pulses, together with the time lag used for the covariance estimates, determine the range resolution of the results [4].

The intensity (magnitude) is a good measure of bubble density, and the Doppler shift (phase) yields an estimate of the radial velocity of the cloud of scatterers. Additional accuracy for the phase estimates (velocity) can be obtained with coded pulses [5-8]. Here this approach is extended to an array of receivers, using digital beam forming of the complex acoustic covariances, and thus providing both intensity and Doppler shift over a continuous sector from each transmission. Additional details are described in [9].

For MBLEX leg 1, the PADS system was oriented so the beam forming is horizontal, covering an area of the surface 25° wide and from 190 to 450 m in range from *Flip*. The intensity images are corrected for attenuation and beam pattern. Values of rms velocity, etc., were found to be insensitive to small changes in the analyzed area. To examine the characteristics and evolution of surface features over the first 40 hours of the storm, the analysis employed every other (even) hour's data from 0800 March 8 to 2300 March 9, 1995, UTC. Over this period, the PADS axis (center-beam) heading was held near 12°T with an active compensation system or "rotator"; this held the heading variations to about 0.1° rms.

B. Scatterer Dynamics

The acoustic backscatter intensity fields approximately correspond to horizontal maps of the vertically integrated content of bubbles near 15 _m radius. The Doppler shift fields represent bubble-weighted vertically averaged radial velocities. It is therefore worthwhile to consider briefly the general behavior of the bubbles.

Conceptually, the bubbles are injected at the surface by breaking waves and are mixed vertically by turbulence: turbulence competes against rise velocity to distribute the bubbles initially. As bubbles are mixed deeper, they are compressed to smaller size and can dissolve (depending on

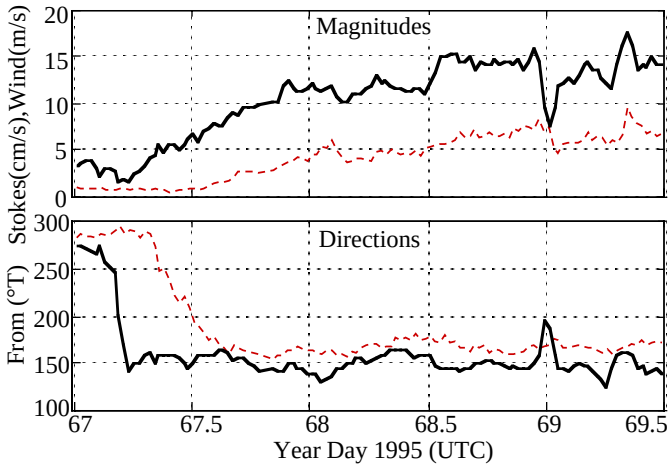

Fig. 2. Wind (solid curve) and Stokes' drift (dashed curve) over the focus time segment of MBLEX leg 1. Note the delay between the onset of wind and development of Stokes' drift. Just prior to this segment, the wind was from the NW, and swell continued to come from that direction, explaining the slow reversal in Stokes' drift direction.

effects such as gas saturation levels, surfactants, etc.). The competing effects are thought to lead to a distribution that is roughly exponential in depth, with a 1 to 1.5 m scale [10]. Significant horizontal variability is also expected, due to both the isolated nature of wave breaking and also to the advection into downwelling zones by larger scale motion such as Langmuir circulation [11-15].

Breaking waves inject bubble clouds that dissipate slowly over several minutes. This should result in a sudden increase in backscattered acoustic intensity at the injection point, with a more gradual decay back to the background level. Because of strong horizontal advection by inertial currents at sea, this signature has proven elusive in previous narrow-beam data sets from the open ocean. Only a few isolated events have been unambiguously identified and painstakingly hand analyzed, and these were from places where inertial currents are small [16]. Intensity information from a 2-D area of the ocean surface should resolve the true temporal evolution of the bubble plumes resulting from breaking waves, avoiding contamination by advection across a narrow beam. In strong winds the breaking events become more common and less isolated and the bubbles might begin to act as tracers of the underlying field of Langmuir circulation. Details of the time-space distribution of bubble clouds in stormy conditions are not yet well known, so there is some interest in examining these distributions per se, and in tracing the evolution from the former isolated injection events to the latter quasi-continuous streaks.

C. Time Averaging and Feature Tracking

The acoustic covariance estimates were averaged over 30 s segments (40 pings) in real time. With advection speeds relative to *Flip* of up to 30 cm/s, this is barely short enough to avoid significant smearing of features by the inertial advection past *Flip* (up to 10 m smearing), but is not long

enough to reduce the surface wave orbital velocities (of the order of 1 m/s) below the size of the mixed layer motions (of the order of 3 cm/s). To attain longer averaging times without smearing the features, a "feature-tracking average" was implemented, using 2-D spatial correlations of each 30-s frame with the next. First, each 30-s average field of acoustic covariances is projected by bilinear interpolation onto a 2 m by 2 m resolution, geometrically corrected, north-aligned grid, using the mean bearing of the sonar system over each 30 s interval. The intensities are used to compute 30-s-lagged spatial correlations. Here, 2-D fast Fourier transforms reduce the computation time by about 100x relative to direct computation, a significant savings for this data volume. The location of the maximum magnitude of each 30-s-lagged spatial correlation yields a two-component Lagrangian velocity estimate, discretized to 0.067 m/s. This is refined by fitting a biquadratic surface to a 5-by-5 grid surrounding the maximum. The result corresponds to an area-mean horizontal advection velocity across the field of view, the "feature-tracking velocity." The accumulated average is shifted by the appropriate offset to align it with the new frame (with bilinear interpolation), and the new acoustic covariance fields are averaged in. The time averaging is roughly exponential, of the form

$$A_n = (1\text{-}1/T)\, A_{n\text{-}1} + (1/T)\, D_n, \qquad (1)$$

with a time constant T = 3 min (or six frames), where the A are averages and D the new data field. The geometrically corrected time-averaged fields of acoustic covariance estimates are then converted to radial velocity (in cm/s, from the phase) and $10*\log_{10}$(intensity) (dB, from the magnitude) and stored for analysis and/or construction of movie sequences. During times of low signal (e.g., early on March 8), this feature tracking process can be unstable. In one instance the feature tracking locked onto a wave-like disturbance moving at about 60 cm/s, probably a high-frequency internal wave packet. Once the wind rose above 2-3 m/s, there were no more such anomalies, and the tracking was robust.

IV. Results

A. Feature versus Doppler velocities: Stokes' drift

The mean velocity derived from the feature-tracking algorithm can be compared to an analogous estimate derived from the Doppler (radial) velocities. The insonified area spans about 12.5° on either side of the center direction (the "axis," aimed toward 12°T over the focus period; e.g., see Plate 2 below). For approximately uniform flow, the along-axis component is given by a cosine-weighted mean, which for this geometry is essentially the area mean. The cross-axis component is given by a sine-weighted mean; this roughly amounts to taking the difference between the means over two much smaller areas and multiplying by 8. The along-axis component is the better determined. The overall agreement between the Doppler and feature-tracking velocity is remarkable, with both velocity time series describing an inertial motion having up to 30 cm/s amplitude over the focus time period (Fig. 3a). Also shown is the velocity jump across the thermocline, estimated by subtracting an average over 35-45 m depth (from the uplooking sonar data) from the surface Doppler-based estimate. In this picture, the decay of the inertial shear is evident (Fig. 3b). In general, such inertial shear is the primary source of energy for mixing in the surface layer [9].

Note that as the sign of the flow relative to *Flip* reverses, the sign of the surface feature velocity minus the Doppler estimate along-axis does not (Fig. 3a, solid lines). There is a steadily increasing unidirectional difference between the two, which roughly parallels the increase in the wind and waves (Fig. 2). In fact, the difference-velocity in the direction along the PADS axis matches the corresponding component of Stokes' drift at the surface (toward 12°T), calculated from the four-wire directional wave array (Fig. 4). For this geometry, the cross-axis differences are too noisy to make a similar judgment. A unique aspect of this comparison is that the Lagrangian (feature) and Eulerian (Doppler) velocities are estimated from the same signal.

The agreement between the Stokes' drift and the difference velocity suggests that the sonar signal arises from a depth which does not vary coherently with wave phase, so

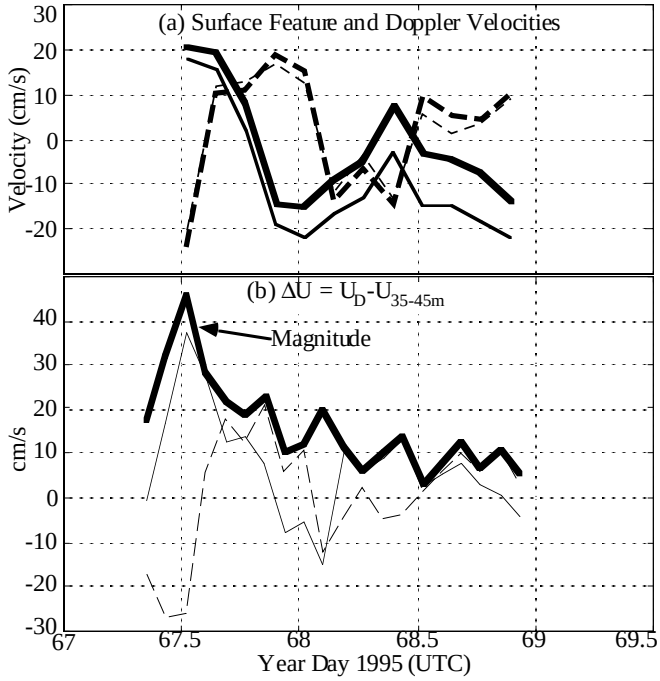

Fig. 3. (a) Mean surface feature velocities (thick lines) versus mean Doppler velocities (thin lines) estimated from the PADS sonar data. The along-axis components (solid lines) are better estimated than the cross-axis (dashed lines); the axis aims toward 12°T. Note the ever-increasing difference between the two along-axis estimates. (b) Net velocity jump across the thermocline, estimated as the difference between the surface Doppler velocities and the mean from the uplooker over 35 m to 45 m depth. The predominant feature in both is an inertial oscillation. Decay of the inertial shear is evident. The magnitude (thick line) of this shear dominates the mixing dynamics.

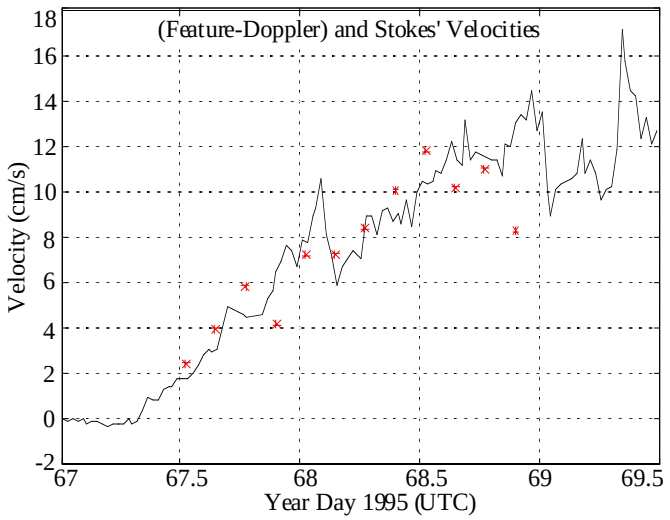

Fig. 4. Comparison of feature-tracking velocities minus Doppler velocities from the sector-scan sonar data (stars) versus Stokes' drift (solid line). Stokes' drift is calculated by linear theory from directional wave-wire data. Only the along-axis component is compared. For this component the net feature-Doppler velocity difference matches the calculated Stokes' drift.

the Doppler shift is an essentially Eulerian measurement of radial velocity. Previously, similar sonar measurements have been interpreted as "semi-Lagrangian," following the bubbles' vertical displacements but not the horizontal [17]. For sound incident at a steeper incident angle on the surface, this interpretation may be valid. These previous measurements were indeed made at steeper angles (from 35 m depth versus 15 m here), but there is no independent evidence by which to judge the interpretation. The transition from semi-Lagrangian to Eulerian behavior versus incident angle would be a study in its own right. In any case, at low grazing angles, as here, the sound rays are excluded from wave crests due to shadowing by the troughs; thus the effective depth of the measurement appears to be a bubble-weighted average from the typical trough depth downward. The bubbles themselves are distributed over several meters, decaying with depth roughly like exp(-z/1.5 m) [10], yielding a centroid of measurement about 1.5 m lower. Thus the effective measurement depth is a meter or two below the wave troughs, which are themselves somewhat below the mean water line.

Conversely, the agreement appears to validate the estimation of Stokes' drift via linear wave theory. The possibility remains that there are errors in both interpretations that cancel. For example, the true Stokes drift could be larger than the linear theory estimate, counterbalanced by underestimation of the net drift from the Feature-Doppler velocity difference.

B. Development of Features

In the early part of the wind event, after the wind begins to rise but before Langmuir circulation is apparent, intensity events suggestive of bubble injection by wave breaking are occasionally seen in the PADS data. Events large enough to be seen clearly against the background variability are rare: about eight events per hour exceed 6 dB above the mean intensity between 1400 and 1900 UTC, March 8. Streaks associated with Langmuir circulation begin to show up after 1900; then it is seen that the larger intensity events tend to occur on a preexisting streak. Visually, whitecapping was common over the whole time period, with every few crests spilling or breaking. Only a small fraction of breaking events produces bubble clouds that stand out. These could be either large but rare "plunging breakers" or coincidental occurrences of reasonably large breakers directly over downwelling zones in the underlying flow. The intensity events become more common as the winds and waves increase.

Streaks associated with Langmuir circulation show up shortly after the appearance of such intensity events and become distinct by about 0000 UTC March 9. In the early hours of March 9 the intensity events begin to look more like sudden enhancements of the streak features themselves. In contrast to the earlier segment, where the intensity events occur as roughly isotropic spots, the later events can be elongated, and sometimes groups of features appear to light up simultaneously over an area several tens of meters on a side. In these cases, the features can appear in adjacent streaks simultaneously (separated by 20 to 40 m). The intensity events appear along previously visible streaks. Throughout this wind event, the streaks are erratic in both time and space, in contrast to the well-aligned features seen previously with a sudden wind "turn-on" event [17] or in lochs or lakes.

C. Scaling of Surface Motion

A measure of the strength of surface motion is the rms surface velocity V^{rms} in cm/s. This was assessed from the data

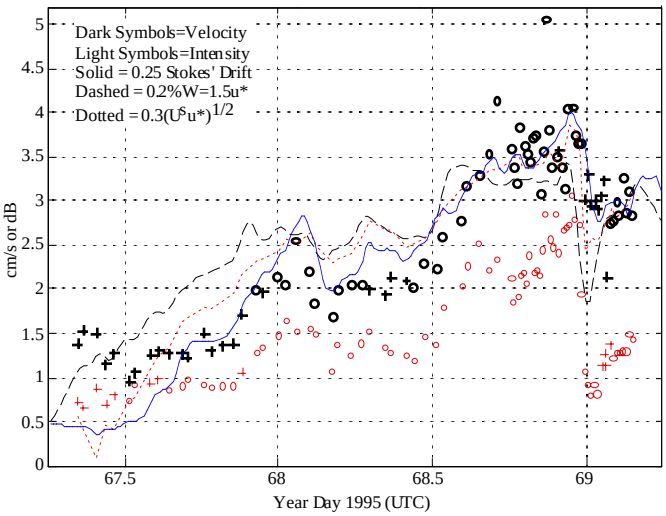

Fig. 5. RMS radial velocity (dark symbols) and intensity (light symbols) associated with the features, versus time. Each symbol represents a half-hour average; crosses represent dubious estimates, circles more reliable ones. For scaling and comparison, $0.25U^S$ (solid line), $0.002W$ (dashed line), and $0.023(U^SW)^{1/2}$ (dotted line) are also shown.

as follows: the data were (1) zero-padded to 256 by 256 points; (2) Fourier transformed in two spatial dimensions; (3) squared; (4) corrected for the simulated response of the array and processing; (4) normalized into power densities. Then (5) a noise estimate was formed from the area between 0.1 and 0.25 fractional power response; (6) the high wavenumbers were masked off where the response drops below 0.25 (13 to 18 m wavelength, depending on orientation); and (7) the noise estimate was subtracted. The square-root of the integral is then the rms velocity.

Do previously suggested scalings for the rms velocity, as measured at the surface, hold in this data set? For the Craik-Leibovich mechanism for generation of Langmuir circulation, the cross-wind velocity fluctuations were expected to scale with either the geometric mean of the wind and Stokes' drift, $(WU^S)^{1/2}$ [18] or with $(W^2U^S)^{1/3}$ [19]. The estimated velocity scale V^{rms}, wind speed W, and Stokes' drift U^S are shown in Fig. 5. The latter two are scaled to provide a reasonable fit to the former over the middle section of the time period. Streaks are first seen after year day 67.66, as the wind exceeds 8 m/s. It is therefore reasonable to restrict the analysis to the time segment after that. The rms surface radial velocities follow the Stokes' drift quite closely from year day 67.66 to the end of the segment, i.e., for winds over 8 m/s.

Scaling of the surface velocities associated with Langmuir circulation can be cast in the general form $V \sim u^* (U^S/u^*)^n$. The value of n is then sought as the slope of the best fit line to $log_{10}(V/u^*)$ versus $log_{10}(U^S/u^*)$ (Fig. 6, circles). Surprisingly, the value n=1 is found, with very little uncertainty (note that U^S/u^* varies over almost an order of magnitude and r^2=0.886; error bounds on the slope are a standard deviation derived by the bootstrap method with 5000 trials [20]. In other words, once the Langmuir circulation is well developed, $V \sim U^S$, and wind stress no longer enters directly in scaling the motion. This surprising result appears to imply a strongly nonlinear influence of the waves on the flow (nonlinear, since a threshold value of wind > 8 m/s must be applied, or, more precisely, a threshold for the existence of well-developed Langmuir circulation).

Earlier reports, using data from the Surface Wave Processes Project (SWAPP), found the above combinations to increase correlations over using wind friction velocity alone [18, 19], but no attempt was made to find an optimal exponent. The SWAPP data were processed with a dual spatial-temporal lag technique to isolate coherent signals while also tracking advection along the beam (see [18] or [19] for details). The data were again corrected for the spatial response of the instruments, estimated from simulated data. Of 4 wind events encountered in SWAPP, only two pass the dual quality controls of (i) a large range of U^S/u^* values and (ii) wind direction remaining uniform. Within each of these, the above fit was again performed (Fig. 6, *'s and +'s). Within each event, the correlation is high; however, the "constant" of proportionality between V^{rms} and U^S varies so much between events that lumping them together makes the correlation vanish (see [21] for details on this comparison).

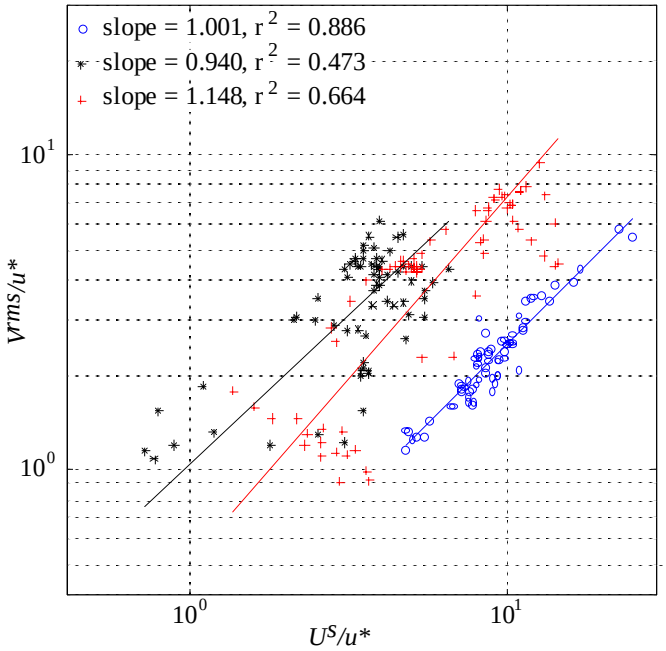

Fig. 6. The empirical fits for n for each "good event" treated separately (o data from MBLEX; * and + from SWAPP). Note that, within each event, the fit is fairly tight. However, the vertical offset of the lines varies significantly between the separate events.

6. Conclusions

The difference between mean feature-tracking and Doppler velocity estimates provides a reasonable and direct estimate of the Stokes' drift near the surface. A unique aspect is that both estimates come from the same data stream, without explicitly resolving the waves. In addition to providing a unique cross-check of calculations of the Stokes' drift from wave data, this may be a dynamically significant parameter for oceanic surface motions.

The rms velocity associated with Langmuir circulation appears to scale tightly with the Stokes' drift alone over the course of individual wind events, rather than with the wind or a combination of wind and waves. This relation is nonlinear in the sense that a threshold must be set for the existence of Langmuir circulation before it holds. Further, the "constant of proportionality" between rms surface velocity and Stokes' drift varies significantly between events. This variation may be related to the ratio of wavelength to mixed layer depth. Dynamic effects of the near-surface bubble layer could also play a role.

References

[1] K. F. Rieder and J. A. Smith, "Removing wave effects from the wind stress vector," *J. Geophys. Res.*, vol. 103, pp. 1363-1374, 1998.

[2] J. A. Smith and K. F. Rieder, "Wave induced motion of FLIP," *Ocean Eng.*, vol. 24, pp. 95-110, 1997.

[3] M. S. Longuet-Higgins, D. E. Cartwright, and N. D. Smith, "Observations of the directional spectrum of sea waves using the motions of a floating buoy," in *Ocean Wave Spectra: Proceedings of a*

Conference, vol. 1, N. A. o. Sciences, Ed. Englewood Cliffs, N.J.: Prentice-Hall, 1963, pp. 111-132.

[4] W. D. Rummler, "Introduction of a new estimator for velocity spectral parameters.," AT&T Bell Labs., Murray Hill, N.J. Rep. MM-68-4141-5, 1968.

[5] J. A. Smith and R. Pinkel, "Improvement of Doppler estimation through repeat sequence coding," in *Oceans '91/Proceedings, October 1-3, 1991, Honolulu, Hawaii, USA/Ocean Technologies and Opportunities in the Pacific for the 90's*, vol. 2. Piscataway, N.J.: IEEE, 1991, pp. 977-984.

[6] R. Pinkel and J. A. Smith, "Repeat-sequence coding for improved precision of Doppler sonar and sodar," *J. Atmos. Oceanic Technol.*, vol. 9, pp. 149-163, 1992.

[7] M. V. Trevorrow and D. M. Farmer, "The use of Barker codes in Doppler sonar measurements," *J. Atmos. Oceanic Technol.*, vol. 9, pp. 699-704, 1992.

[8] B. H. Brumley, R. G. Cabrera, K. L. Deines, and E. A. Terray, "Performance of a broad-band acoustic Doppler current profiler," *IEEE J. Oceanic Eng.*, vol. 16, pp. 402-407, 1991.

[9] J. A. Smith, "Evolution of Langmuir circulation during a storm," *Journal of Geophysical Research*, vol. 103, pp. 12,649-12,668, 1998.

[10] C. B. Crawford and D. M. Farmer, "On the spatial distribution of ocean bubbles," *J. Geophys. Res.*, vol. 92, pp. 8231-8243, 1987.

[11] L. Zedel and D. Farmer, "Organized structures in subsurface bubble clouds - Langmuir circulation in the open ocean," *J. Geophys. Res.*, vol. 96, pp. 8889-8900, 1991.

[12] S. A. Thorpe, "On the clouds of bubbles formed by breaking wind waves in deep water, and their role in air-sea gas transfer.," *Philos. Trans. R. Soc. London, Ser. A*, vol. 304, pp. 155-210, 1982.

[13] S. A. Thorpe, "Bubble clouds: A review of their detection by sonar, of related models, and of how K_V may be determined.," in *Oceanic Whitecaps and Their Role in Air-Sea Exchange Processes*, E. C. M. a. G. M. Noicall, Ed. Norwell, Mass.: D. Reidel, 1986, pp. 57-68.

[14] S. Vagle, W. G. Large, and D. M. Farmer, "An evaluation of the WOTAN technique of inferring oceanic winds from underwater ambient sound," *J. Atmos. Oceanic Technol.*, vol. 7, pp. 576-595, 1990.

[15] D. Farmer and M. Li, "Patterns of bubble clouds organized by Langmuir circulation," *J. Phys. Oceanogr.*, vol. 25, pp. 1426-1440, 1995.

[16] S. Thorpe and A. J. Hall, "The characteristics of breaking waves, bubble clouds, and near-surface currents observed using side-scan sonar," *Cont. Shelf Res.*, vol. 1, pp. 353-384, 1983.

[17] J. A. Smith, "Observed growth of Langmuir circulation," *J. Geophys. Res.*, vol. 97, pp. 5651-5664, 1992.

[18] A. J. Plueddemann, J. A. Smith, D. M. Farmer, R. A. Weller, W. R. Crawford, R. Pinkel, S. Vagle, and A. Gnanadesikan, "Structure and variability of Langmuir circulation during the surface waves processes program," *J. Geophys. Res.*, vol. 101, pp. 3525-3543, 1996.

[19] J. A. Smith, "Observations of Langmuir circulation, waves, and the mixed layer," in *The Air Sea Interface: Radio and Acoustic Sensing, Turbulence, and Wave Dynamics*, M. A. Donelan, W. H. Hui, and W. J. Plant, Eds. Toronto, Ont.: Univ. of Toronto Press, 1996, pp. 613-622.

[20] Diaconis and B. Efron, "Computer-intensive methods in statistics," *Sci. Am.*, vol. 248, pp. 116-130, 1983.

[21] J. A. Smith, "Doppler sonar observations of Langmuir circulation," in *Air-sea Fluxes of Momentum, Heat, and Chemicals*, G. Geernaert, Ed. Dordrecht, the Netherlands: Kluwer Academic Publishers, 1998, pp. (in press).